Laser transmission–backscattering through inhomogeneous cirrus clouds

Szu-Cheng Ou, Yoshihide Takano, Kuo-Nan Liou, Randy J. Lefevre, and Michael W. Johnson

We have developed a two-dimensional (2D) model for inhomogeneous cirrus clouds in plane-parallel and spherical geometries for the analysis of the transmission and backscattering of high-energy laser beams. The 2D extinction-coefficient and mean effective ice-crystal size fields for cirrus clouds can be determined from a combination of the remote sensing of cirrus clouds by use of the Advanced Very High Resolution Radiometer on board National Oceanic and Atmospheric Administration satellites and the vertical profiling of ice-crystal size distributions available from limited measurements. We demonstrate that satellite remote sensing of the position and the composition of high cirrus can be incorporated directly in the computer model developed for the transmission and backscattering of high-energy laser beams in realistic atmospheres. The results of laser direct transmission, forward scattering, and backscattering are analyzed carefully with respect to aircraft height, cirrus cloud optical depth, and ice-crystal size and orientation. Uncertainty in laser transmission that is due to errors in the retrieved ice-crystal size is negligible. But uncertainty of the order of 2% can be produced if the retrieved optical depth has errors of ± 0.05. With both the aircraft and the target near the cloud top, the direct transmission decreases, owing to the propagation of the laser beam through the curved portion of the cloud top. This effect becomes more pronounced as the horizontal distance between the aircraft and the target increases.

OCIS codes: 010.3310, 010.1320, 290.1090, 280.0280.

1. Introduction

With advances in laser technology in recent years, high-energy lasers at near-infrared wavelengths have been developed and incorporated into an aircraft platform for engagement with a moving target. For such an active system to be effective in operation, atmospheric effects must be carefully taken into consideration. The presence of persistent high-altitude cirrus clouds along the path between the aircraft platform and the target, particularly in the typical cirrus-residing regions of the upper troposphere and the lower stratosphere, can significantly affect the transmission and backscattering of laser beams.

In a paper previously published in this journal,[1] a near-infrared airborne-laser transmission model for thin cirrus clouds was developed on the basis of the successive-order-of-scattering approach to account for the multiple scattering of randomly and horizontally oriented ice crystals associated with an aircraft–target system. Direct transmission and the transmission that is due to multiple scattering were formulated specifically for a homogeneous plane-parallel geometrical system, in which scattering and absorption associated with aerosols, water vapor, and air molecules were accounted for. A number of sensitivity experiments were performed for the investigation of effects of aircraft–target position, cirrus cloud optical depth, and ice-crystal size on laser transmission for tactical applications. We illustrated that transmission contributions produced by orders of scattering higher than 1 are small and can be safely neglected. The possibility of horizontal orientation of ice crystals could enhance the transmission of laser beams in the aircraft–target geometry. The transmitted energy is strongly dependent on the horizontal distance between the aircraft and the target and on the cloud optical depth, as well as on whether the cloud is above or below the aircraft.

S. C. Ou (ssou@atmos.ucla.edu), Y. Takano, and K. N. Liou are with the Department of Atmospheric Sciences, University of California, Los Angeles, Los Angeles, California 90095-1565. R. J. Lefevre and M. W. Johnson are with the Airborne Laser Program System Office, Kirtland Air Force Base, New Mexico 87117-6612.

Received 4 February 2002; revised manuscript received 24 June 2002.

0003-6935/02/275744-11$15.00/0

Satellite mapping of the optical depth in midlatitude and tropical regions has illustrated that cirrus clouds are frequently finite in nature and display substantial horizontal variability.[2,3] Vertical inhomogeneity of the ice-crystal size distribution and ice–water content has also been demonstrated by balloon-borne replicator sounding observations,[4] as well as the time series of backscattering coefficients derived from lidar and radar returns.[5–7] To quantify laser transmission and backscattering with reasonable accuracy, it is necessary to take into account the horizontal and vertical variations of cirrus cloud structure. In this paper, because most of the laser energy is confined in the vertical plane defining the aircraft and the target, we construct a two-dimensional (2D) inhomogeneous cirrus cloud model for the simulation of laser transmission and backscattering, employing the successive-order-of-scattering method. The effects of the Earth's curvature on the laser transmission and backscattering have also been taken into account in this study. The direct transmission, forward scattering, and backscattering are subject to the variation of the extinction coefficient and the mean effective ice-crystal size along the line of sight between the laser and the target. For the input to the laser transmission–backscattering model, 2D cirrus cloud fields are constructed from the mapping of the horizontal distribution of ice–water content and mean effective ice-crystal size of cirrus clouds by use of National Oceanic and Atmospheric Administration–Advanced Very High Resolution Radiometer (NOAA–AVHRR) data.

The arrangement of this paper is as follows. Section 2 presents the model formulation for the laser transmission and backscattering. In Section 3 we discuss the physical significance of computational results, in which 2D and one-dimensional model calculations of laser transmission and backscattering energy are compared for aircraft above, within, and below the cloud and for selected optical depths and mean effective ice-crystal sizes. Effects of uncertainty of satellite-retrieved optical depths and ice-crystal sizes on laser transmission and backscattering are further analyzed. Finally, a summary is given in Section 4.

2. Formulation of Laser Transmission–Backscattering

A. Transmission–Backscattering in a Two-Dimensional Plane-Parallel Geometry

Our transmission formulation associated with multiple scattering follows transmission models developed by Liou *et al.*[1,8] In general, transmission that is due to the first-order scattering, i.e., the forward scattering, is relatively small compared with the directly transmitted radiation but is nevertheless significant. As stated earlier in Section 1, transmission contributions produced by the second-order scattering are much smaller than those of the direct component and can be neglected. For what follows, we consider the direct transmission and the forward scattering and backscattering that are due to the first-order scattering in a 2D plane-parallel atmosphere. In the rest of this paper, the terms forward scattering and backscattering refer to the first-order scattering only.

The direct transmission through an inhomogeneous cirrus cloudy atmosphere follows the rule of exponential attenuation and can be written in terms of the transmitted power F_d in the form

$$\begin{aligned} F_d &= F_0 \exp[-(\beta_{\mathrm{nc,a}} v + \beta_{\mathrm{nc,b}} u)] \exp\left(- \int_0^s \beta_e \mathrm{d}s' \right) \\ &= F_0 \exp[-(\beta_{\mathrm{nc,a}} v + \beta_{\mathrm{nc,b}} u)] \\ &\quad \times \exp\left[- \int_0^s (\beta_{\mathrm{air}} + \beta_{\mathrm{aer}} + k_v \rho + \beta_{\mathrm{cld}}) \mathrm{d}s' \right], \end{aligned} \quad (1)$$

where F_0 is the laser power in watts and the total extinction coefficient β_e is the integration of the scattering coefficient of air molecules β_{air}, the extinction coefficient of aerosols β_{aer}, the absorption coefficient of water vapor times water-vapor density $k_v\rho$, and the extinction coefficient of cirrus cloud particles β_{cld} over the path along the laser beam. In reference to Fig. 1(a), the parameter s' is the distance EB along the laser beam between a certain point at height z in the cloud and the cloud base, which can be expressed by

$$s' = (z - z_b)/\mu, \quad (2)$$

where μ is the sine of the scan angle $\theta = \tan^{-1}[(z_a - z_m)/d]$ of the laser beam. The parameter s is a distance along the laser beam between the cloud top and the cloud base that can be expressed by

$$s = (z_t - z_b)/\mu. \quad (3)$$

The parameters z_a, z_t, z_b, and z_m are heights of the aircraft, cloud top, cloud base, and target, respectively; d is the horizontal distance between the aircraft and the target; $u = (z_b - z_m)/\mu$ denotes a distance BM between the cloud base and the target; and $v = (z_a - z_t)/\mu$ denotes a distance AT between the aircraft and the cloud top. Exponential attenuation outside the cloud is also accounted for in Eq. (1), where $\beta_{\mathrm{nc,a}}$ and $\beta_{\mathrm{nc,b}}$ are extinction coefficients that are due to noncloud species (air molecules, aerosols, and water vapor) above and below the cloud, respectively.

Forward scattering can be expressed in the form

$$\begin{aligned} F^{(1)}(0, \Omega) &= \exp[-(\beta_{\mathrm{nc,a}} v + \beta_{\mathrm{nc,b}} u)] \int_0^s J^{(1)}(s', \Omega) \\ &\quad \times \exp\left[- \int_0^{s'} \beta_e(s'') \mathrm{d}s'' \right] \beta_e(s') \mathrm{d}s'. \end{aligned} \quad (4)$$

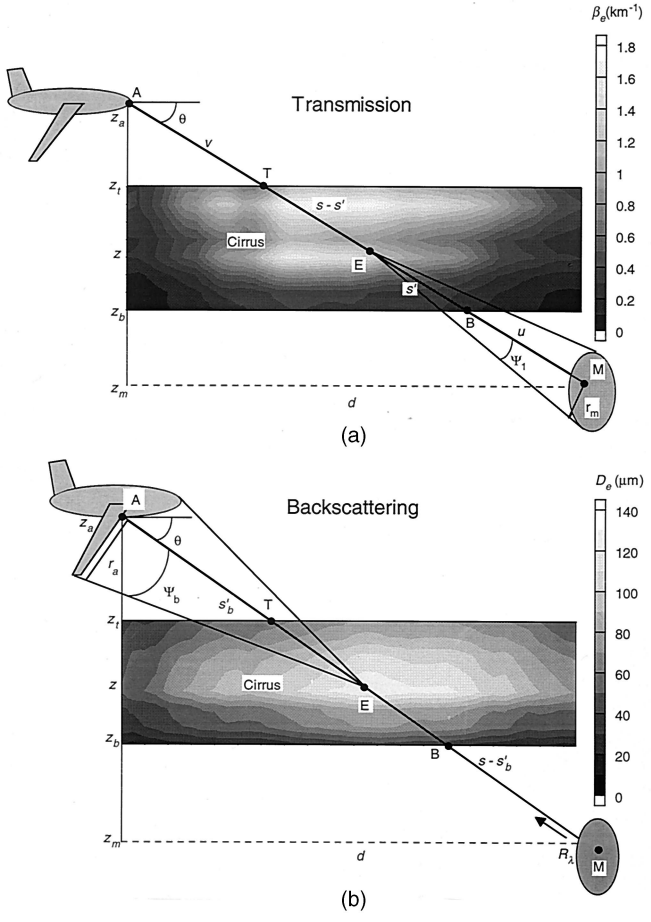

Fig. 1. (a) Laser transmission through a 2D inhomogeneous cirrus cloud. A gray-scale contour inside the cirrus shows a distribution of relative extinction coefficient β_e (km^{-1}). $s' = EB$, $s - s' = ET$, $u = BM$, $v = AT$. (b) Laser backscattering through a 2D inhomogeneous cirrus cloud. A gray-scale contour inside the cirrus shows a distribution of effective particle size D_e (μm). $s - s_b' = EM$, $s_b' = EA$.

On the basis of the principle of the successive order-of-scattering approach, the first-order source function $J^{(1)}(s', \Omega)$ can be formulated in the form

$$J^{(1)}(s', \Omega) = \frac{\varpi(s')}{2} F^{(0)}(s', \Omega) \int_0^{\Psi_1} P_{\text{cld}}(\Theta) \sin \Theta \, d\Theta, \tag{5}$$

where $\varpi(s')$ is the single-scattering albedo, which is a function of s', and $P_{\text{cld}}(\Theta)$ is the phase function of the cloud particle, which is a function of the scattering angle Θ. We consider only the cloud phase function, $P_{\text{cld}}(\Theta)$ because the diffracted intensity is more intense by more than 3 orders of magnitude than those of aerosols and air molecules. Ψ_1 is an angle associated with the target when it is viewed from point E, defined by

$$\Psi_1 = \tan^{-1}\left(\frac{r_m}{u + s'}\right), \tag{6}$$

where r_m is the effective radius of the target. The directly transmitted power at s' is given by

$$F^{(0)}(s', \Omega) = F_0 \exp\left[-\int_{s'}^{s} \beta_e(s'') ds''\right]. \tag{7}$$

In this formulation, the laser beam is assumed to be collimated.

In a manner similar to the transmission formulation and in reference to Fig. 1(b), the source function that is due to the first-order backscattering based on the successive-order-of-scattering approach can be expressed in the form

$$J^{(1)}(s_b', \Omega) = \frac{\varpi(s')}{2} F^{(0)}(s_b', \Omega) \int_{\pi - \Psi_b}^{\pi} P_{\text{ave}}(\Theta) \sin \Theta \, d\Theta, \tag{8}$$

where the angle

$$\Psi_b = \tan^{-1}(r_a / s_b'), \tag{9}$$

in which r_a is an effective radius of the aircraft and s_b' is the distance between the aircraft and a certain point along the path connecting the aircraft and the target, as shown in the schematic diagram depicted in Fig. 1(b). The direct transmission in this case is given by

$$F^{(0)}(s_b', \Omega) = F_0 \exp\left[-\int_{s'}^{s_b'} \beta_e(s'') ds''\right]. \tag{10}$$

In Eq. (8) the terms $P_{\text{ave}}(\Theta)$ and β_e denote the average phase function and the average extinction coefficient defined by

$$P_{\text{ave}}(\Theta) = \frac{[h(z - z_b) - h(z - z_t)]\beta_{s,\text{cld}} P_{\text{cld}}(\Theta) + \beta_{s,\text{aer}} P_{\text{aer}}(\Theta) + \beta_{\text{air}} P_{\text{air}}(\Theta)}{[h(z - z_b) - h(z - z_t)]\beta_{s,\text{cld}} + \beta_{s,\text{aer}} + \beta_{\text{air}}}, \tag{11}$$

$$\beta_e = [h(z - z_b) - h(z - z_t)]\beta_{\text{cld}} + \beta_{\text{aer}} + \beta_{\text{air}} + k_v \rho, \tag{12}$$

where $h(z - z')$ denotes a step function, which is defined as $h(z - z') = 1$ for $z \geq z'$; otherwise, $h(z - z') = 0$. The order of magnitude for the phase function in the backscattering direction is approximately the same for ice crystals, air molecules, and aerosols ($\sim$0.1), so that $P_{\text{ave}}(\Theta)$ is used. And because of the comparative magnitude of the backscattering phase functions, aerosol particles above, below, and inside

the cloud can make an important contribution to backscattering in contrast to transmission. Finally, the first-order backscattering is given by

$$F_b^{(1)}(0, \Omega) = \int_0^{s} J^{(1)}(s_b', \Omega) \times \exp\left[-\int_{s'}^{s_b'} \beta_e(s'')\mathrm{d}s'' \right] \beta_e(s_b')\mathrm{d}s_b'. \quad (13)$$

Furthermore, reflection from the target can be accounted for in the backscattering formulation as follows:

$$F_{\mathrm{ref}} = R_\lambda T^2 F_0(\pi r_a^2/s_b^2), \quad (14)$$

where R_λ is the reflectivity of the target, T ($=F_d/F_0$) is the transmittance between the aircraft and the target, F_0 is the laser power, s_b is the distance along the laser beam between the aircraft and the target, and $\pi r_a^2/s_b^2$ is the effective solid angle by which the target sees the aircraft.

B. Transmission–Backscattering in a Two-Dimensional Spherical Geometry

In this subsection, we present only the formulation for the geometry in which both the aircraft and the target are above the cloud, as illustrated in Fig. 2. The direct transmission of a laser beam in a 2D spherical geometry is similar to Eq. (1) and can be expressed by

$$F_d^* = F_d F_s, \quad (15)$$

where F_d is the direct transmission based on a plane-parallel geometry. Referring to Fig. 2(a), when both the aircraft and the target are above the cloud, the direct transmission through the cloud, F_s, is now defined by

$$F_s = \exp\left[-\int_0^{s^*} \beta_e(s')\mathrm{d}s' \right], \quad (16)$$

where s^* is the distance along the laser beam between the two cloud interception points, T_1 and T_2, and s' is the distance along the laser beam between a point in the cloud and the far-side intercept, T_2 [see Fig. (2a)].

Forward scattering is the sum of forward scattering based on a plane-parallel geometry, $F^{(1)}(0, \Omega)$, plus forward scattering in the cloudy atmosphere that is due to the spherical geometry:

$$F^{*(1)}(0, \Omega) = F^{(1)}(0, \Omega) + F_s^{(1)}(0, \Omega). \quad (17)$$

On the basis of the successive order-of-scattering approach, the second term is given by

$$F_s^{(1)}(0, \Omega) = \int_0^{s^*} J^{(1)}(s', \Omega) \times \exp\left[-\int_0^{s'} \beta_e(s'')\mathrm{d}s'' \right] \beta_e(s')\mathrm{d}s'. \quad (18)$$

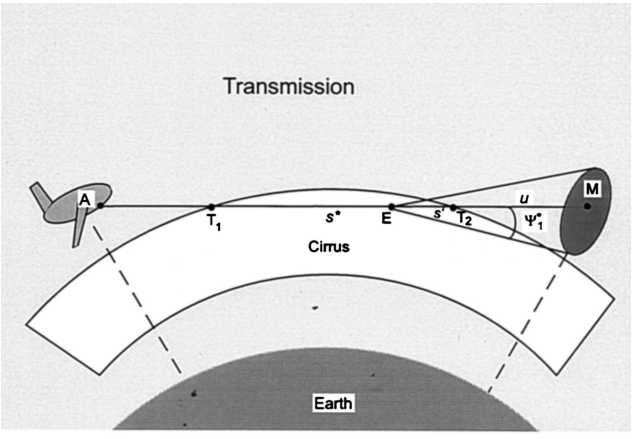

(a)

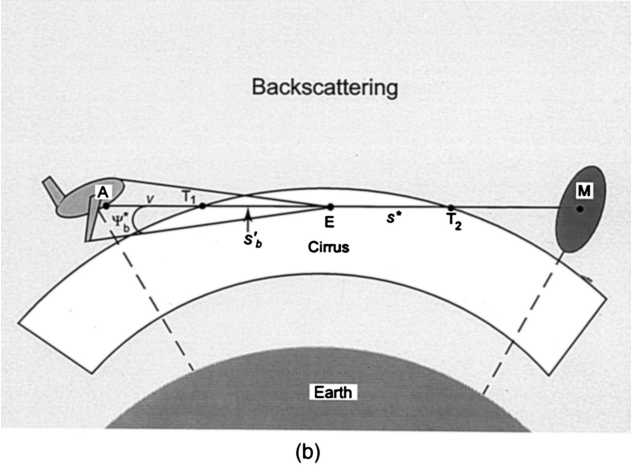

(b)

Fig. 2. Schematic diagram (a) for laser transmission and (b) for laser backscattering through a spherical cirrus cloud. $s^* = T_1T_2$, $s' = ET_2$, $u = T_2M$, $s_b' = ET_1$, $v = T_1A$.

The source function $J^{(1)}(s', \Omega)$ in Eq. (18) can be written in the form

$$J^{(1)}(s', \Omega) = \frac{\varpi(s')}{2} F^{(0)}(s', \Omega) \int_0^{\Psi_1^*} P(\Theta)\sin\Theta\mathrm{d}\Theta, \quad (19)$$

where the angle

$$\Psi_1^* = \tan^{-1}\left(\frac{r_t}{s' + u} \right) \quad (20)$$

and the direct transmission term is given by

$$F^{(0)}(s', \Omega) = F_0 \exp\left[-\int_0^{s^*-s'} \beta_e(s'')\mathrm{d}s'' \right]. \quad (21)$$

Likewise, laser backscattering that is due to the first-order scattering in a 2D spherical geometry is the sum of two terms defined in the following:

$$F_b^{*(1)}(0, \Omega) = F_b^{(1)}(0, \Omega) + F_{sb}^{(1)}(0, \Omega), \quad (22)$$

where $F_b^{(1)}(0, \Omega)$ is the first-order backscattering for the plane-parallel case and $F_{sb}^{(1)}(0, \Omega)$ is an additional

contribution from the spherical geometry involving cirrus clouds. On the basis of the geometry defined in Fig. 2(b), the latter can be expressed by

$$F_{sb}^{(1)}(0, \Omega) = \int_0^{s^*} J_b^{(1)}(s_b', \Omega) \times \exp\left[-\int_0^{s_b'} \beta_e(s'')\mathrm{d}s'' \right] \beta_e(s_b')\mathrm{d}s_b'. \quad (23)$$

From the geometry, the source function that is due to the first-order scattering can be expressed in the form

$$J_b^{(1)}(s_b', \Omega) = \frac{\varpi(s_b')}{2} F^{(0)}(s_b', \Omega) \int_{\pi-\Psi_b^*}^{\pi} P_{\mathrm{ave}}(\Theta)\sin\Theta\mathrm{d}\Theta, \quad (24)$$

where the angle

$$\Psi_b^* = \tan^{-1}\left(\frac{r_a}{s_b' + v} \right), \quad (25)$$

in which v is the distance between the aircraft and the cloud top along the laser beam. However, the direct transmission is given by

$$F^{(0)}(s_b', \Omega) = F_0 \exp\left[-\int_{s'}^{s_b'} \beta_e(s'')\mathrm{d}s'' \right]. \quad (26)$$

Because of the sphericity of the cirrus cloud top, the contribution that is due to direct reflection from the target differs from that given in Eq. (14). It is given by

$$F_{\mathrm{ref}}^* = R_\lambda T_s^2 F_0(\pi r_a^2/s_b^2), \quad (27)$$

where

$$T_s = F_d F_s / F_0. \quad (28)$$

In the case in which the aircraft or the target is located below the cloud top, a separate set of equations similar to Eqs. (15)–(28) can be formulated but will not be duplicated here.

3. Computational Results

Input to the transmission–backscattering model includes the single-scattering and absorption parameters for hexagonal ice crystals and aerosols and the correlated absorption coefficients for water vapor. The determination of these input parameters has been described by Liou *et al.*[1] The required background atmospheric temperature, pressure, and humidity profiles, as well as aerosol profiles, are assumed for the purpose of this study. To evaluate the attenuation of laser energy through high thin cirrus clouds, geometrical and system parameters must be prescribed. The geometrical parameters include the horizontal distance between the aircraft and the target (d); heights of the aircraft (z_a), cloud top (z_t), and base (z_b); and initial and final target heights. The system parameters include the wavelength (λ), the reflectivity of the target, and the equivalent radii of the target (r_m) and of the aircraft (r_a). In what follows, we present illustrative results computed from the laser transmission and backscattering model. We first examine effects of aerosol and water-vapor scattering–absorption and of ice-crystal shape on the first-order laser backscattering, assuming that the cloud is homogeneous. We then compare results of model calculations of laser transmission and backscattering for homogeneous and inhomogeneous clouds as well as for plane-parallel and spherical geometries.

Consider the aircraft above the cloud as illustrated in Fig. 1(b). The first-order backscattered and target-reflected powers reaching the aircraft are shown in Fig. 3 as functions of the target height. The top and bottom panels show effects of aerosols and water vapor and of cloud particle size, respectively. The left and right panels are for the vertical optical depth of 0.05 and 0.2, respectively. Other input parameters are $\lambda = 1.315\ \mu\mathrm{m}$, $F_0 = 10^6\ \mathrm{W}$, $r_m = 3\ \mathrm{m}$, $R_\lambda = 0.2$, $r_a = 4\ \mathrm{m}$, $d = 100\ \mathrm{km}$, $z_a = 11\ \mathrm{km}$, $z_t = 9.5\ \mathrm{km}$, and $z_b = 9\ \mathrm{km}$. The lightly shaded strip signifies the vertical extent of the cloud, and the triangle depicts the position of the aircraft. The first-order backscattering is almost independent of the target height. For a scattering point E far away from the aircraft, the angle Ψ_b subtended from E by the aircraft is smaller [Fig. (1b)], whereas aerosols and air molecules exist close to the aircraft so that the angle Ψ_b for these particles is larger. As a result, the backscattering source function $J^{(1)}$, which is due to the cloud particles and which is a measure of the contribution to the backscattering reaching the aircraft, also becomes smaller [see Eqs. (8) and (9)]. Thus the backscattered power determined from Eq. (13) is dominated by the scattering of air molecules and enhanced by additional aerosol scattering near the aircraft. For this reason, it is essentially constant, regardless of the cloud optical depth or the location of the target. Moreover, the target-reflected power is much smaller than the first-order backscattering. As the target leaves the surface, the attenuated target reflection increases owing to reduced water-vapor absorption. As the target approaches the cloud base, the attenuated target reflection decreases owing to an increasing cloud path-integrated optical depth, i.e., the integrated optical depth along the path. Effects of the cloud particle size are negligibly small, whereas the reflection from the target through larger cloud particles is increased owing to their smaller attenuation.

For the aircraft within the cloud, the backscattered power as a function of the target height is shown in Fig. 4. Except for the aircraft height, all other input parameters are the same as those specified for Fig. 3. Because the scattering coefficient of ice particles is much larger than those of aerosols and air molecules, the first-order backscattering is dominated by the scattering contribution of cloud particles near the aircraft, and its magnitude is 1 to 2 orders larger than that displayed in Fig. 3. The effect of absorption by

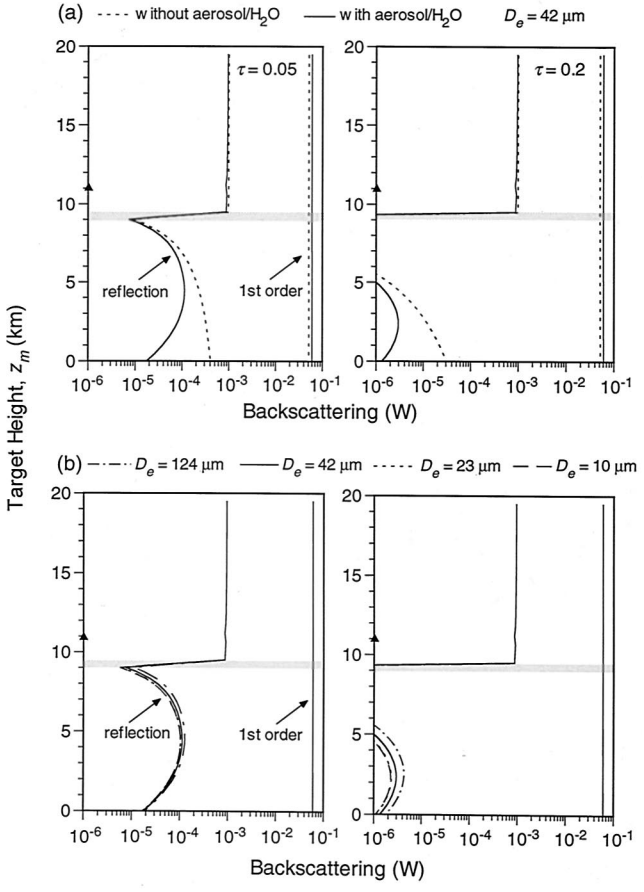

Fig. 3. Backscattered power that is due to the first-order scattering and the reflection from the target. (a) Upper panels show effects of aerosols and water vapor. (b) Lower panels show effects of cloud particle size. The assumed conditions are as follows: $\lambda = 1.315$ μm, $F_0 = 10^6$ W, $r_m = 3$ m, $R_\lambda = 0.2$, $r_a = 4$ m, $d = 100$ km, $z_a = 11$ km, $z_t = 9.5$ km, and $z_b = 9$ km.

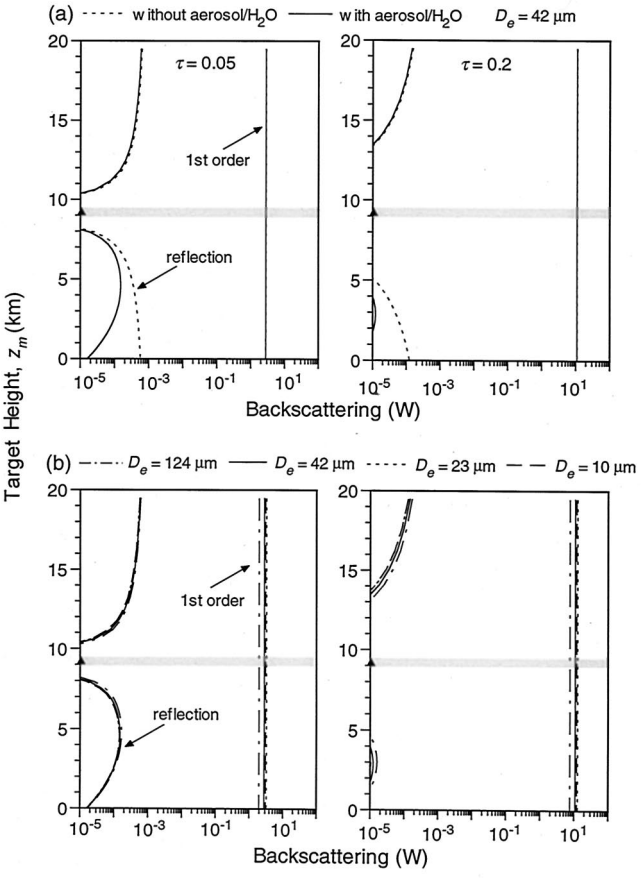

Fig. 4. Same as Fig. 3, except that the aircraft is within the cloud ($z_a = 9.25$ km).

water vapor on the reflection from the target is significant, particularly when the target is below the cloud, as shown in the top panels of Fig. 4. The first-order backscattering for a mean effective ice-crystal size $D_e = 124$ μm is the smallest among the four different values, as shown in the bottom panels of Fig. 4, because phase function values for this size in the range of scattering angles between $\pi - \Psi_b$ and π are the smallest among the four.

Figure 5 shows the comparison of backscattered power for three-dimensional (3D) randomly oriented hexagonal ice crystals, equal-area spheres, Parry columns (randomly oriented columns in the horizontal plane), and 2D plates (randomly oriented plates in a horizontal plane). The aircraft is immediately above ($z_a = 9.6$ km, higher than the cloud top by only 0.1 km) and within ($z_a = 9.25$ km) the cloud, and all other parameters are the same as those used in Figs. 3 and 4. For the aircraft above the cloud, the backscattered power decreases as the target height increases, as illustrated in the top panels of Fig. 5(a). This is because the aircraft is close to the cloud top, so that the first-order backscattering is dominated by the scattering of cloud particles, and effects of aerosols and air molecules are relatively small. Owing to the glory peak in the phase function for equal-area spheres, the backscattered power for equal-area spheres is larger than that for 3D randomly oriented hexagonal ice crystals. Because of the relatively smaller extinction coefficient caused by the horizontal orientation of 2D plates, the backscattered power for 2D plates is smaller than that for 3D randomly oriented hexagonal ice crystals.

For the aircraft within the cloud, the first-order backscattering by 3D randomly oriented hexagonal ice crystals is slightly larger than that by equal-area spheres, as shown in Fig. 5(b). This is because the solid angle Ψ_b can become large when the aircraft is inside the cloud and because the complementary angle in the required integration, $\pi - \Psi_b$, is out of the maximum glory region. Because of the smaller extinction coefficient and therefore the smaller optical depth in the case of 2D plates under the configuration of the present aircraft–target geometry, the first-order backscattered power is smaller than those of randomly oriented ice crystals and Parry columns. In addition, when the target height z_m is close to the aircraft height z_a, specular reflection that is due to 2D plates enhances the backscattered power, as illustrated in Fig. 5(b) by the small bulge within the cloud.

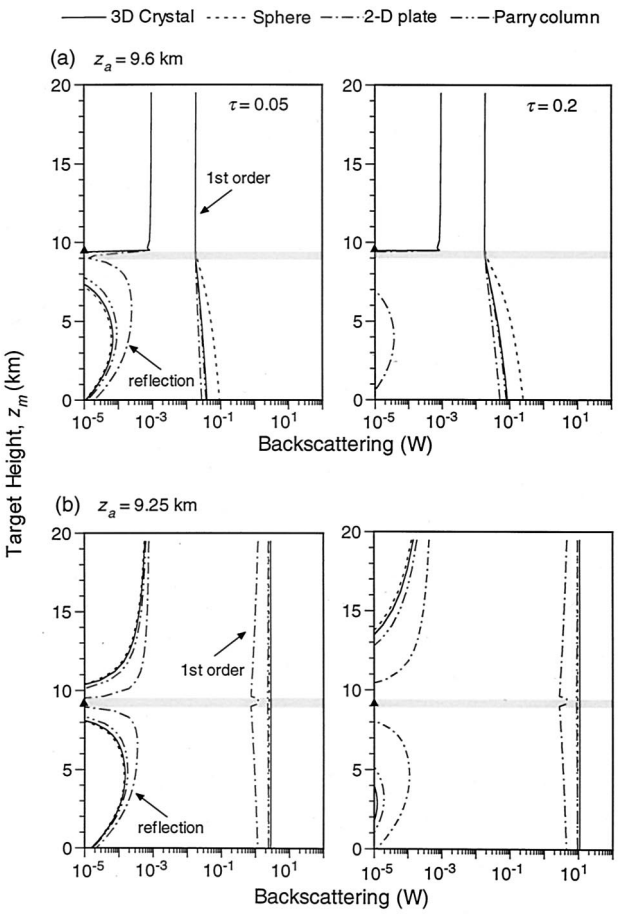

Fig. 5. Backscattered power that is due to the first-order scattering and the reflection from the target. Each panel shows effects of cloud particle shape and orientation and aircraft height: (a) aircraft at 9.6 km and (b) aircraft at 9.25 km. $\lambda = 1.315$ μm, $D_e = 42$ μm, $F_0 = 10^6$ W, $r_m = 3$ m, $R_\lambda = 0.2$, $r_a = 4$ m, $d = 100$ km, $z_t = 9.5$ km, and $z_b = 9$ km.

To investigate effects of the cloud inhomogeneity, we first constructed 2D fields for ice–water content and mean effective ice-crystal size of cirrus clouds on the basis of optical depths and mean effective ice-crystal sizes derived from the AVHRR data. In our previous study, we developed a retrieval algorithm utilizing the 0.63–3.7-μm reflectance–radiance correlation technique for the inference of cirrus cloud optical depth and mean effective ice-crystal size (Ou *et al.*[9]). Although the 3.7-μm radiance includes both solar reflection and the thermal emission components, this algorithm does not require the removal of either component and thus is more straightforward and applicable than algorithms involving adjustments of the 3.7-μm radiance. The adding–doubling radiative transfer program[10] has been used to generate look-up tables of 0.63-μm reflectances and 3.7-μm radiances. We employ 14 optical depths ranging from 0.125 to 12. We also use six representative ice-crystal sizes described in Rao *et al.*[11] This algorithm has been applied to AVHRR data that were collected during the FIRE-II Intensive Field Operations field experiment, which was held between late November and early December 1991 at Coffeyville, Kansas. Validation of this algorithm has been carried out by use of the cloud microphysics data sampled by the balloon-borne replicator and airborne 2D probes that were collocated and coincident with the AVHRR measurements. We demonstrated that the retrieved cirrus cloud optical depths and mean effective sizes compare reasonably well with those determined from *in situ* analyses.

To characterize the cirrus cloud field for the present transmission model calculations, we selected a cirrus case that occurred in the northern Oklahoma area on 18 April 1997, during which AVHRR data from the NOAA-14 satellite and collocated and coincident *in situ* cloud microphysics measurements were available. The ranges of the solar zenith, satellite viewing, and relative azimuth angles were 35–40°, 5–30°, and 25–30°, respectively. A 0.4° × 2.0° domain (36.4–36.8 °N and 96.5–98.5 °W) was selected for the retrieval purpose. The horizontal distribution of the retrieved optical depths and mean effective ice-crystal sizes exhibited substantial variability. Following the procedure outlined in Liou and Rao,[12] we constructed 3D extinction-coefficient and mean effective ice-crystal size fields on the basis of the satellite-retrieved cloud parameters. Subsequently, the extinction coefficient and ice-crystal size in 2D space can be obtained as inputs to the laser transmission model. This observation-based 2D inhomogeneous model is a first approximation to real inhomogeneous clouds. The 2D inhomogeneous cloud will be extended to a 3D inhomogeneous cloud model.

Figure 6 shows the direct transmission and forward scattering and backscattered powers for the 1.315-μm laser beam as functions of the target height. In this calculation, the spatially averaged 2D cloud optical depth field was scaled down to 0.1 and 0.4 to simulate thin cirrus situations. The horizontal optical depths for these two cases (~8 and 32) are close to that for $\tau = 0.05$ and 0.2 with $d = 100$ km (~10 and 40), as specified for Figs. 3–5, because the present horizontal distance d is 40 km. Here the horizontal optical depth denotes the optical depth along the path, when the aircraft is located around the cloud top, and the target is located around the cloud base. The mean effective ice-crystal size used is 74 μm, based on the domain average of the retrieved mean effective sizes. The vertical extent of the cloud is between 7.5 and 11.1 km, corresponding to the maximum cloud thickness observed by the ground-based radar. The aircraft is placed at 11.2 km, immediately above the cloud top, because backscattering for this aircraft altitude is the most sensitive to the target height. When the target rises to 4 km, the direct transmission for the inhomogeneous cloud is larger than that for the homogeneous cloud because the laser beam path-integrated optical depth is smaller for an inhomogeneous cloud, as shown in Fig. 1(a). When the target rises above 4 km and before reaching the cloud base, the direct transmission is smaller for an inhomogeneous cloud because

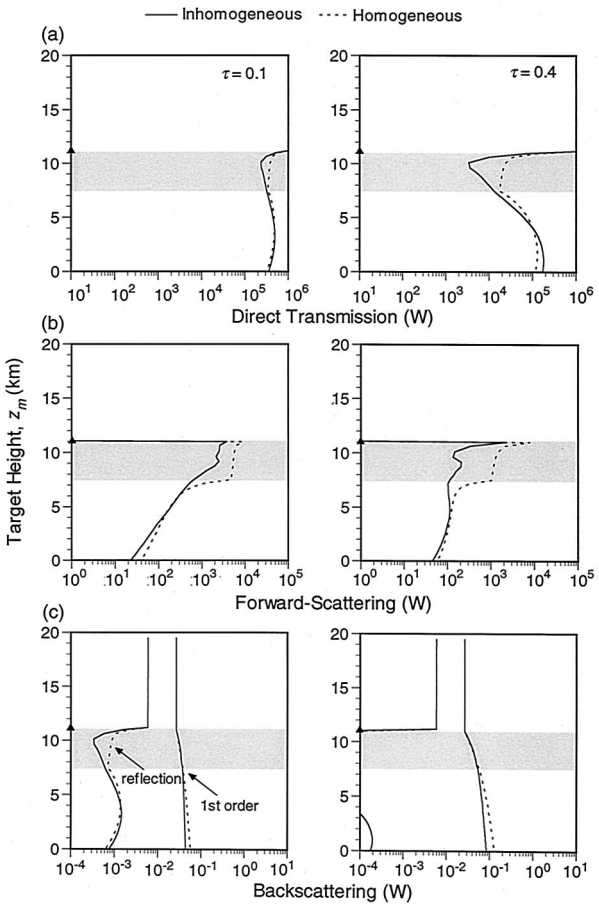

Fig. 6. Direct transmission, forward scattering, and backscattering in an inhomogeneous and a homogeneous cirrus clouds with the same optical depth. $\lambda = 1.315$ μm, $D_e = 74$ μm, $F_0 = 10^6$ W, $r_m = 3$ m, $R_\lambda = 0.2$, $r_a = 4$ m, $d = 40$ km, $z_a = 11.2$ km, $z_t = 11.1$ km, and $z_b = 7.5$ km.

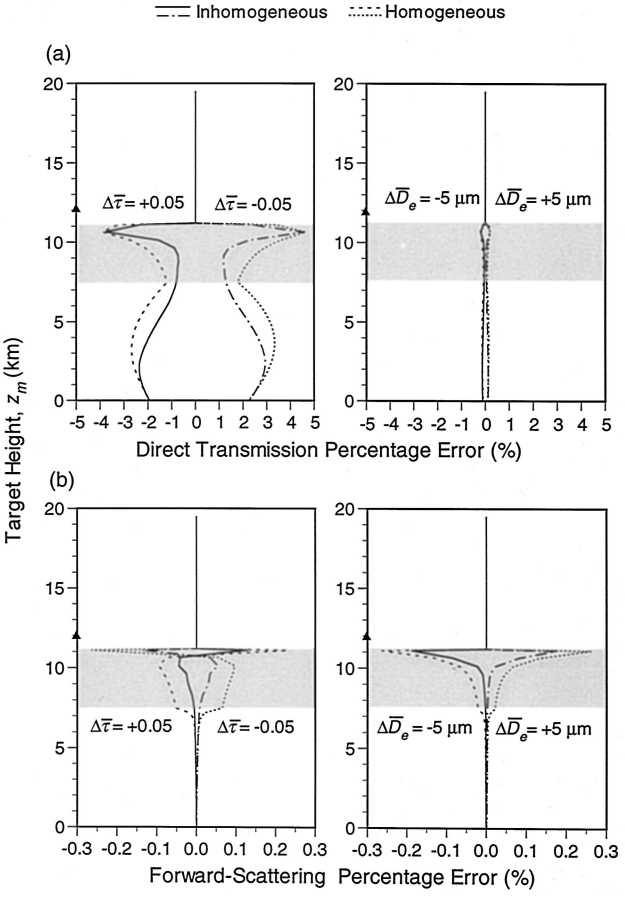

Fig. 7. Percentage errors in the direct transmission and forward scattering that are due to uncertainties in the cloud optical depth (±0.05) and in the mean effective size (±5 μm) as functions of the target height. $\tau = 0.4$. Other conditions are the same as for Fig. 6.

the laser beam path length is larger for an inhomogeneous cloud, as also shown in Fig. 1(a). When the target is in the cloud, both the direct transmission and the forward scattering are larger for the homogeneous case than for the inhomogeneous case. This is due to the larger laser beam path length and larger ice-crystal size in the case of the inhomogeneous cloud (see Fig. 1). The first-order backscattering is almost the same for the target within the cloud in both cases. Moreover, when the target is below the cloud, the cloud inhomogeneity has little effect on the laser transmission and backscattering.

Figure 7 shows effects of satellite retrieval uncertainties in the cloud optical depth and mean effective size on laser transmission as functions of the target height for inhomogeneous and homogeneous clouds. Again, the aircraft is assumed to be above the cloud. The cloud optical depth and mean effective size used were 0.4 and 74 μm, respectively. Uncertainties in the retrieved cloud optical depth are set to be ±0.05, and for the cloud mean effective size they are ±5 μm. These are typical error ranges for satellite retrievals of cloud optical depth and mean effective size.[10] The resulting errors in laser transmission are expressed as $\Delta W/F_0$, where ΔW is the difference between the perturbed and the unperturbed laser powers and F_0 is the initial laser power.

For direct transmission, errors that are due to the optical depth uncertainties of ±0.05 in the computed laser power occur when the target is within and below the cloud. The error that is due to uncertainty in cloud optical depth is less than 4%. Local maximum values of error occur near the surface and the cloud top. Because direct transmission follows the rule of exponential attenuation, $\exp(-\tau^*)$, where τ^* is the cloud optical depth along the laser beam path, the differential of the direct transmission, dF_d, which is proportional to the error of the direct transmission, also follows the rule of exponential attenuation, i.e., $\Delta W \propto dF_d \propto -\exp(-\tau^*)d\tau^*$. As the target leaves the surface, the errors increase initially because the optical depth of the laser beam path decreases owing to the decrease in atmospheric water-vapor absorption. As the target rises above 2 km, the errors decrease because effects of cloud attenuation become dominant.

Once the target enters the cloud, the optical depth of the laser beam path begins to decrease, so that

errors increase steadily toward a maximum value corresponding to the target at the cloud top. Finally, after the target departs the cloud, the direct transmission is no longer subject to errors in cloud retrievals, and errors drop to zero. Errors are larger for homogeneous clouds than for inhomogeneous clouds because the optical depth of the laser beam path is smaller for the former. However, the pattern of variation for both cases is similar.

For the forward-scattering contribution, errors that are due to the optical depth uncertainties of ± 0.05 in the computed laser power occur when the target is within and below the cloud. The error that is due to uncertainty in the cloud optical depth is less than 0.2%, much smaller than that for the direct transmission. Local maximum errors occur near the cloud top. Because the forward-scattering contribution to laser transmission is proportional to the product of the exponential attenuation term and the optical depth, i.e., $F^{(1)} \propto \exp(-\tau^*)\tau^*$ [see Eq. (4)], the differential of the forward-scattering contribution term, $dF^{(1)}$, which is proportional to the error of the forward scattering, also follows the rule of exponential attenuation, i.e., $\Delta W \propto dF^{(1)} \propto \exp(-\tau^*)(1 - \tau^*)d\tau^*$. As the target leaves the surface, and before it reaches the cloud top, the optical depth is larger than 1. Errors are dominated by the exponential term and are negatively correlated with the term $(1 - \tau^*)d\tau^*$. However, right at the cloud top, the optical depth drops close to zero, and errors in this case are proportional to $d\tau^*$ and have maximum or minimum values. The magnitude of errors for homogeneous clouds is larger than for that for inhomogeneous clouds because the optical depth of the laser beam path is smaller for the former, leading to a larger value of $\exp(-\tau^*)(1 - \tau^*)$.

For both direct transmission and forward scattering, errors that are due to the mean effective size uncertainty of ± 5 μm in the computed laser power are less than 0.3%. Local maximum errors occur near the cloud top. As discussed in Liou *et al.*,[1] direct transmission depends weakly on the mean effective size through the term $\exp[-\beta_e(1 - f_\delta)]$, where f_δ is the fractional energy that resides in the forward direction of the phase function. The term $(1 - f_\delta)$ decreases when the mean effective size increases, leading to the increase in the exponential term and in the direct transmission. Forward scattering also depends on the mean effective size. Because the diffraction peak is sharply confined to forward-scattering directions for larger mean effective sizes [see Eq. (5)], errors in forward scattering are positive for a positive error in mean effective sizes. In addition, because forward scattering is proportional to the exponential attenuation term, the magnitude of errors increases with target height, reaching a maximum near the cloud top.

Figure 8 shows effects of uncertainties in the satellite retrievals of cloud optical depth and mean effective size on laser backscattering. Although the magnitude of errors in backscattering is generally much smaller than that for direct transmission, there are still many interesting features. When the target

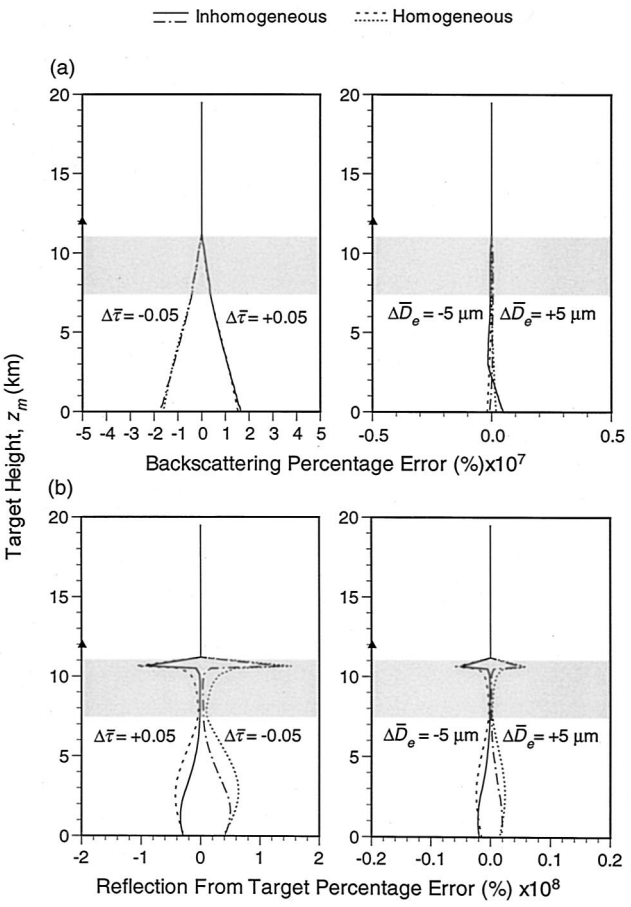

Fig. 8. Percentage errors for the first-order backscattering and the reflection from the target that are due to uncertainties in the cloud optical depth (± 0.05) and in the mean effective size (± 5 μm) as functions of the target. The conditions are the same as for Fig. 6.

leaves the surface, the incident point of the laser beam at the cloud top is close to the aircraft. This point shifts away from the aircraft as the target rises, and effects of aerosol scattering and water-vapor absorption become dominant, so that the absolute value of backscattering errors decreases as shown in the upper-left panel. The reflection from the target is proportional to the square of direct transmission. The lower-left panel of Fig. 8 shows a shape similar to that in the upper-left panel of Fig. 7. When the mean effective size D_e is approximately 74 μm, $P(\Theta = 180°)$ increases with an increase of D_e. Backscattering increases (decreases), owing to a perturbation of $\Delta D_e = \pm 5$ μm, as shown in the upper-right panel. However, the sign is reversed near the ground for the inhomogeneous cirrus. The effective size D_e is 40–50 μm around the cloud top under the aircraft, as shown in Fig. 1(b). $P(180°)$ locally decreases from $P(180°, D_e = 42\ \mu m) = 0.256$ to $P(180°, D_e = 48\ \mu m) = 0.225$. The reversal of sign around $z_m = 0$ can be understood in terms of the local maximum of $P(180°)$ at 42 μm.

Finally, effects of the spherical Earth on direct transmission, forward scattering, and backscattering

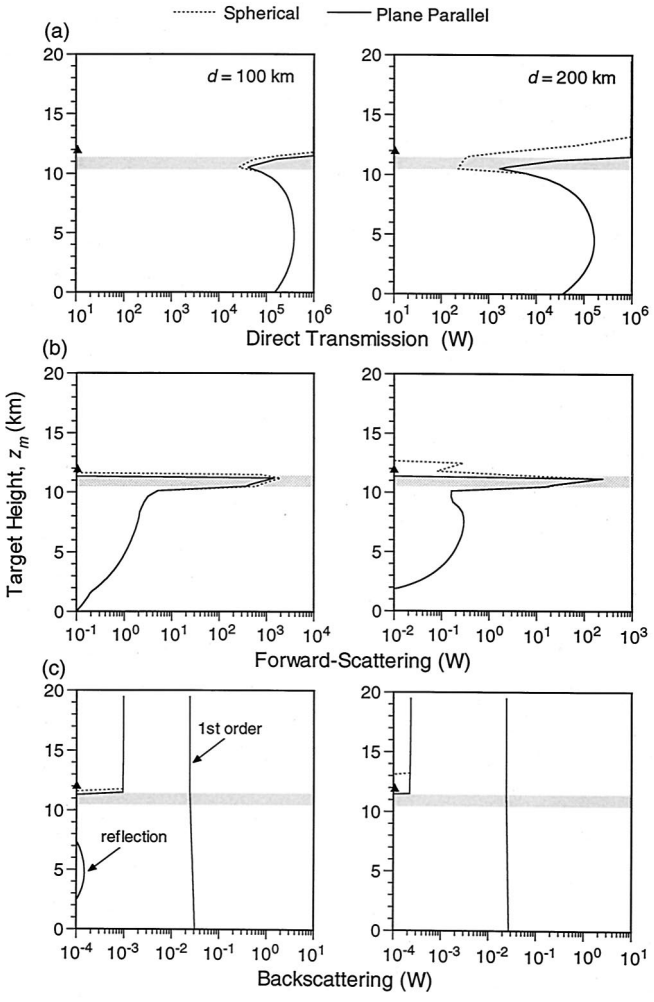

Fig. 9. Direct transmission, forward scattering, and backscattering in a spherical atmosphere and a plane-parallel atmosphere. $\lambda = 1.315$ μm, $D_e = 42$ μm, $F_0 = 10^6$ W, $\tau = 0.05$, $r_m = 3$ m, $R_\lambda = 0.2$, $r_a = 4$ m, $z_a = 12$ km, $z_t = 11.5$ km, and $z_b = 10.5$ km.

are shown in Fig. 9. Two values of the horizontal distance [$d = 100$ km (left panels) and 200 km (right panels)] between the aircraft and the target were specified. Clouds are assumed to be homogeneous and located between 10.5 and 11.5 km with $\tau = 0.05$. The aircraft is located above the cloud at 12 km. For the direct transmission, the effect of the spherical Earth is more significant for $d = 200$ km than for $d = 100$ km, particularly for a target height between the cloud base and the aircraft altitude. Direct transmission powers for spherical and plane-parallel atmospheres are virtually the same for the target below the cloud base. However, for $d = 200$ km, as an extreme case, the direct transmission for the spherical geometry is smaller than that for the plane-parallel geometry by approximately a factor of 10 for the target near the cloud base and by approximately a factor of 10^3 for the target near the cloud top because the cloud path length is longer for spherical geometry. The difference in the forward scattering between the two geometries is again negligible for the target below the cloud. The forward scattering is larger for spherical geometry by approximately 100 W for the target near the cloud top. The additional forward scattering $F_s^{(1)}$ is proportional to the product of the exponential attenuation term and the optical depth, $F_s^{(1)} \propto \exp(-\tau^*)\tau^*$ [Eq. (18)]. When the target is immediately above the cloud top, $F_s^{(1)}$ increases with an increase of the target height owing to the exponential attenuation term. When the target rises higher, $F_s^{(1)}$ decreases because of the domination of the linear optical depth term over the exponential attenuation term. For this reason, there is a secondary peak for $F_s^{(1)}$ above the cloud top at approximately 12.5 km for $d = 200$ km, as shown in the middle right panel of Fig. 9. Because the effect of the scattering of cloud particles is weaker than those of the scattering of aerosols and air molecules, the Earth's curvature has little effect on first-order backscattering for aircraft at some distance above the cloud top. However, because of the effect of the Earth's curvature, reflection from the target is reduced for the same reason that the direct transmission shows a reduction, as illustrated in the top panel.

4. Summary

We have developed a computer model for computing laser transmission, forward scattering, and backscattering through 2D inhomogeneous thin cirrus clouds in both plane-parallel and spherical geometry based on the successive-order-of-scattering approach. We first examine effects of aerosol and water-vapor scattering–absorption and of ice-crystal shape on the first-order laser backscattering, assuming the cloud is homogeneous. For an aircraft above the cloud, the first-order backscattering is essentially constant, regardless of the target height or cloud composition. For an aircraft within the cloud, the first-order backscattering varies with the cloud optical depth but is nearly constant with respect to the target height. Reflection from the target that reaches the aircraft is generally 2 to 6 orders of magnitude less than the first-order backscattering. We also compared backscattering from different shapes of ice crystals. The backscattered power for 3D randomly oriented hexagonal ice crystals is smaller than that for equal-area spheres, owing to the glory peak in the phase function for equal-area spheres. Also, because of the relatively smaller extinction coefficient caused by the horizontal orientation of 2D plates, the backscattered power for 2D plates is smaller than that for 3D randomly oriented hexagonal ice crystals.

To simulate the inhomogeneous thin cirrus cloud situation, we used the AVHRR data along with collocated and coincident *in situ* ice microphysics measurements for a cirrus cloud case to construct a 3D extinction coefficient and mean effective size fields following a procedure that was developed by our research group. The 2D cloud fields were subsequently obtained by the averaging of respective cloud parameter fields in the north–south direction for use in the laser transmission model. Results of the direct transmission, forward scattering, and backscat-

tering of a laser beam through homogeneous and inhomogeneous clouds are compared for aircraft above and within the cloud and for selected optical depths and mean effective sizes. It is shown that cloud inhomogeneity affects the laser transmission and backscattering owing to differences in the integrated optical depths along the line of sight.

Moreover, we investigated the effects of uncertainty in the satellite-retrieved optical depths and ice-crystal sizes on laser transmission computations. We found that uncertainty in laser transmission produced by errors in the retrieved ice-crystal sizes is negligible. However, uncertainty of the order of 2% could result from errors in the retrieved optical depth of ± 0.05. Finally, we studied the effects of the spherical Earth on the laser transmission and backscattering through thin cirrus clouds. When the aircraft is near the cloud top and the target is located at or immediately above the cloud top, the direct transmission decreases significantly owing to the propagation of the laser beam through the curved portion of the cloud top. The magnitude of this decrease becomes more significant as the horizontal distance between the aircraft and the target increases. The present results at the wavelength of 1.315 μm can be readily applied to another near-infrared wavelength (e.g., 1.03 μm).

This research has been supported by U.S. Air Force Office of Scientific Research grant F49620-01-1-0057.

References

1. K. N. Liou, Y. Takano, S. C. Ou, and M. W. Johnson, "Laser transmission through thin cirrus clouds," Appl. Opt. **39,** 4886–4894 (2000).
2. P. Minnis, K. N. Liou, and Y. Takano, "Inference of cirrus cloud properties using satellite observed visible and infrared radiance. Part I: Parameterization of radiance field," J. Atmos. Sci. **50,** 1279–1304 (1993).
3. S. C. Ou, K. N. Liou, Y. Takano, N. X. Rao, Q. Fu, A. J. Heymsfield, L. M. Miloshevich, B. Baum, and S. A. Kinne, "Remote sounding of cirrus cloud optical depths and ice crystal sizes from AVHRR data: verification using FIRE-II-IFO composite measurements," J. Atmos. Sci. **52,** 4143–4158 (1995).
4. L. M. Miloshevich and A. J. Heymsfield, "A balloon-borne continuous cloud particle replicator for measuring vertical profiles of cloud microphysical properties: instrument design, performance, and collection efficiency analysis," J. Atmos. Ocean. Technol. **14,** 753–768 (1997).
5. K. Sassen, "The polarization lidar technique for cloud research: a review and current assessment," Bull. Am. Meteorol. Soc. **72,** 1848–1886 (1991).
6. J. D. Spinhirne and W. D. Hart, "Cirrus structure and radiative parameters from airborne lidar and spectral radiometer observations: the 28 October 1986 FIRE study," Mon. Weather Rev. **118,** 2329–2343 (1990).
7. G. G. Mace, T. Ackerman, P. Minnis, and D. F. Young, "Cirrus layer microphysical properties derived from surface-based millimeter radar and infrared interferometer data," J. Geophys. Res. **103,** 23207–23216 (1998).
8. K. N. Liou, Y. Takano, S. C. Ou, A. Heymsfield, and W. Kreiss, "Infrared transmission through cirrus clouds: a radiative model for target detection," Appl. Opt. **29,** 1886–1896 (1990).
9. S. C. Ou, K. N. Liou, M. D. King, and S. C. Tsay, "Remote sensing of cirrus cloud parameters based on a 0.63–3.7 μm radiance correlation technique applied to AVHRR data," Geophys. Res. Lett. **26,** 2437–2440 (1999).
10. Y. Takano and K. N. Liou, "Radiative transfer in cirrus clouds. II. Theory and computation of multiple scattering in an anisotropic medium," J. Atmos. Sci. **46,** 20–36 (1989).
11. N. X. Rao, S. C. Ou, and K. N. Liou, "Removal of the solar component in AVHRR 3.7-μm radiances for the retrieval of cirrus cloud parameters," J. Appl. Meteorol. **34,** 481–499 (1995).
12. K. N. Liou and N. X. Rao, "Radiative transfer in cirrus clouds. IV. Cloud geometry, inhomogeneity, and absorption," J. Atmos. Sci. **53,** 3046–3065 (1996).